Proceedings of Global Power and Propulsion Society
ISSN-Nr: 2504-4400
GPPS Xi'an21
18th–20th October, 2021

www.gpps.global

GPPS-TC-2021-0360

High fidelity finite element model updating and deviation characterization method for geometric mistuned bladed disks

Daosen Liang
Chongqing University
20156130@cqu.edu.cn
Chongqing, China

Rui Zhang
Chongqing University
20166092@cqu.edu.cn
Chongqing, China

Yulin Wu
Chongqing University
1793438389@qq.com
Chongqing, China

Zichu Jia
Chongqing University
zichuj@cqu.edu.cn
Chongqing, China

Zhifu Cao
Chongqing University
aezfcao@cqu.edu.cn
Chongqing, China

Jianyao Yao
Chongqing University
yaojianyao@cqu.edu.cn
Chongqing, China

ABSTRACT

To accurately obtain the influence of geometric deviation on the vibration characters of the bladed disk. It is necessary to count the deviation characteristics of a large number of real bladed disks and establish the high-fidelity structural analysis model. An automatic finite element model updating method of mistuned blade disks and characterization method of blade geometric deviation is proposed in this paper. The geometric mistuning blade finite element model is obtained by moving the finite element structured mesh nodes to the measured point cloud data. The proposed finite element model updating method includes bladed disk cloud processing, blade surface classification, blade node movement. The method can be applied to large deformed blades and damaged blades. The obtained geometric deviation can accurately distinguish the abnormal blade model. The surface measurement data of the blade is obtained by a blue light optical scanner. Compare with the blade modal experiments result, the updated high-fidelity finite element calculation result error was less than 8‰.

INTRODUCTION

High cycle fatigue (HCF) damage to the blade can be incurred by the vibration of the bladed disk . Reports show that more than three quarters of all aero-engine failures account for HCF damage. Theoretically, The blade and the disc are structures with rotational cyclic symmetry. If each blade-disk sector is considered to be identical, then the cyclic theory symmetry can be used to evaluate the dynamics of the whole structure based on one fundamental sector of the disk blade. However, due to geometric machining errors, material dispersion, wear and damage, there are small differences between the structural characteristics of each blade, which can break the cyclic symmetry of the blade disc structure, usually called mistuning. The vibration of the bladed disks is extremely sensitive to mistuning, the response of the blades can magnified sererl times Martel and Corral (2009). To determine the impact of mistuning on balded disks, require use of the high-fidelity modelling consider blade mistuning to analyze.

In the Finite element model (FEM) analysis, there are several methods to account for bladed disk mistuning. The proportional mistuning method (PMM) is to modify the Young's modulus or the corresponding stiffness matrix of each rotor blade until the finite element model can predict the measured natural frequency of the actual rotor blade Castanier and Pierre (2006)Laxalde et al. (2007). PMM only changes the material properties in the finite element parameters, and not need to consume massive computational resources. However, blade mistuning should also include changes in geometry due to wear, damage, etc. Geometric mistuning methods (GMM) changes both the stiffness and mass distribution of the blade model, and its vibration characteristics are significantly different from those of PMM in some cases. And the reliability of PMM is limited to a small frequency range. Therefore, the blade geometry deviations due to manufacturing and damaged need to be factored into the FEM of the bladed disk.

There are two types of blade accurate measurement methods: the contact and non-contact methods. The quantification of geometric deviations are mainly by using the contact measuring machine to obtain the coordinates of each blade section of an engineering blsk. The advantage of the contact measurement method is the high accuracy of measurement, especially

the leading and trailing edge of the blade which has the aerodynamic properties of the more significant influence. However, the efficiency of contact methods is poor, only obtain a few cross-sectional coordinates data, and a large number of points on the blade surface cannot be measured. In contrast, the non-contact optical measurement has become the main method to measure the bladed disks surface, which is faster and more convenient, more adaptable, and has a larger amount of measured point cloud data (PCD) than contact measurementHarding (2005). Kaszynski tested that the accuracy of non-contact optical measurement can reach 2.5 μm, but its measurement repeatability and accuracy are not high at locations with a small radius of curvature such as the leading edge trailing edge. Voiget, Hogner combined industrial CT and optical measurement methods to obtain geometric information of the turbine blade surface and internal cooling holes and to build the parametric blade modelVoigt et al. (2019).

After measuring the blade, the obtained point cloud data were processed into a triangular surface mesh as shown in Fig. 2. In order to reflect the effect of geometric uncertainty in the simulation model and consider the real blade mistuning form, require to move the finite element nodes to the triangular mesh surface to establish a high-fidelity finite element model. In high-fidelity finite element modeling, Kaszynski and Beck established a modeling method from CAD to CAE based on the accurate measurement of geometric mistuning blade Kaszynski et al. (2014). And the transformation from nominal model to high-fidelity geometric mistuning model was realized by finite element mesh deformation, and the effects of modeling accuracy such as point cloud density and measurement noise were investigated. Finally, the accuracy of the finite element model is verified by modal tests and the response under traveling wave excitation Kaszynski et al. (2015) .

The method allows the mesh quality after the deformation of the blade mesh to be evaluated and smoothed by the defined mass function. Backhaus compared two design methods considering wear, manufacturing uncertainty and investigated the accuracy of numerical digitization of blade section airfoil modeling and blue light projection system for 3D-Coordinate-measuring machine Backhaus, Maywald, Schrape, Voigt and Mailach (2017)Backhaus, Harding, Schrape, Voigt and Mailach (2017).

Excessive blade deformation caused by wear and damage factors is common. But the above methods are no longer general for large deformation mistuning blades, but only for smaller degrees of geometrical mistuning. In this paper, a generalized high-fidelity modeling method for geometrical mistuned bladed disks is proposed for damaged, large-deformed blades, and the accuracy of the proposed algorithm is verified by comparing the realistic bladed disks modal test results with the deformed finite element modal Analysis results. The blade deviation data is determined by the displacement of each node in three XYZ directions when obtaining a high-fidelity finite element model. The blade geometric deviations are correspondingly very complex and highly random, which are difficult to be accurately described in a simple form, and this high dimensional uncertainty brings great difficulties to analyze mistuning characteristics of the balde disks.

METHODOLOGY

0.1 Blade geometry deviation characterization

Currently, the characterization methods of stochastic geometric deviations mainly use the principal component analysis(PCA) method, whereby the modalities of geometric deviations are obtained, which can describe complex geometric deviation distributions with fewer parameters by means of linear superpositionHenry et al. (2016)Boyd (2019).

Assuming that the blade node degrees of freedom are p, the geometric deviation of each degree of freedom is , and the number of samples is n, the following dataset is generated.And PCA is the combination of p observed variables by linear transformation into p new variables,

$$\mathbf{X} = \begin{bmatrix} x_{11} & x_{12} & \cdots & x_{1p} \\ x_{21} & x_{22} & \cdots & x_{2p} \\ \vdots & \vdots & \vdots & \vdots \\ x_{n1} & x_{n2} & \cdots & x_{ip} \end{bmatrix} = \begin{bmatrix} \mathbf{X}_1 & \mathbf{x}_2 & \cdots & \mathbf{X}_p \end{bmatrix} \tag{1}$$

$$\begin{cases} F_1 = a_{11}X_1 + a_{12}X_2 + \ldots + a_{1p}X_p \\ F_2 = a_{21}X_1 + a_{22}X_2 + \ldots + a_{2p}X_p \\ F_p = a_{p1}X_1 + a_{p2}X_2 + \cdots + a_{pp}X_p \end{cases} \tag{2}$$

PCA obtains an optimal set of unit orthogonal bases by performing covariance operations on the original data set. The linear combination of the obtained bases is used to reconstruct the original sample space to satisfy that the mean square error between the reconstructed samples and the original space samples is the minimum value

$$m = \frac{1}{n\sum_{i=1}^{n} x_i} \tag{3}$$

$$S = \frac{1}{n\sum^{n} x_i \left(x_i - m\right)\left(x_i - m\right)^T} \tag{4}$$

$$SW = W\Lambda \tag{5}$$

where m is mean vector, S is covariance matrix. $W = (w_1, w_2, \cdots, w_n)$, $\Lambda = \mathrm{diag}(\lambda_1, \lambda_2, \cdots, \lambda_n)$, w is the eigenvector, $\Lambda =$ is the eigenvalue.

0.2 High fidelity finite element model updating method

The flow chart for constructing the high-fidelity model in this paper is shown in Fig1.

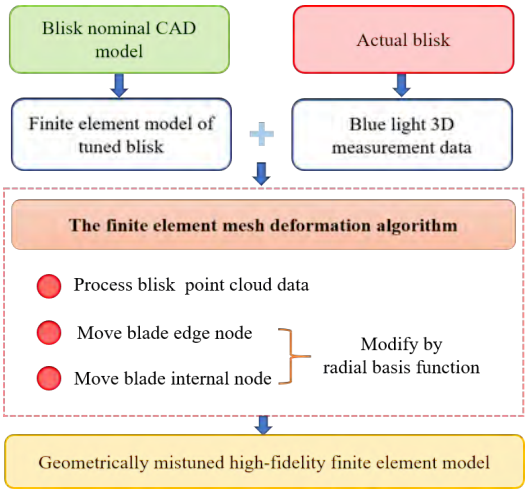

Figure 1 High fidelity finite element model updating method flowchart

According to the nominal CAD model of bladed disk to obtain the symmetry finite element model. The blisk point cloud data (PCD) is obtained by measuring the actual engineering blisk structure with an optical scanning instrument and is composed of coordinate points and triangles connecting these points. The mistuned finite element model is provided by moving the symmetry finite element model node to blisk PCD.

0.2.1 Blisk point cloud processing

The blisk PCD measured by optical measurement does not have the common reference frame with the nominal CAD model. Calculate the rigid body transformation according to the rotation matrix and the translation matrix, and use the gradient descent method to minimize the distance between the blisk PCD and the FEM external nodes.

$$\min_{\theta} \|\theta\|_0 \text{ s.t. } \theta = C_{FEM} - C_{PCD}R^T - T \tag{6}$$

where the R and T are the rotation matrix and translation matrix, C_{FEM} is the FEM nodes coordinates and C_{PCD} is the point cloud data coordinates.

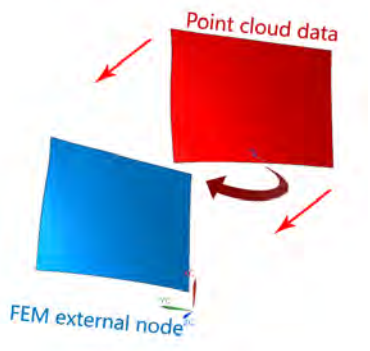

Figure 2 Blade surface points alignment

After align blisk PCD, execute the boolean operation on the blisk surface's point cloud data and split it into two parts: the disc and the blades. Next, identify each blade from the overall blades PCD. In the overall blade PCD, each blade is a separate individual (there is no triangle connection between different blades). Using the above rules, a point is randomly selected from the overall blades PCD, and the connecting point is found and iterated until there is no connected point, then individual blade PCD can be identified. Since the initial blade PCD is randomly selected, the position of each blade PCD

cannot be determined. Calculate the angle between the vector of the blade PCD center of gravity and the central axis, and sort blades according to the angle of 0 360° to the blades for each position.

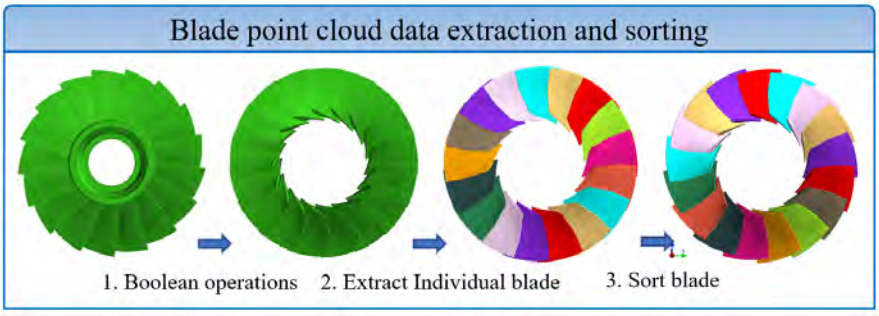

Figure 3 Blade points cloud data extraction and sorting

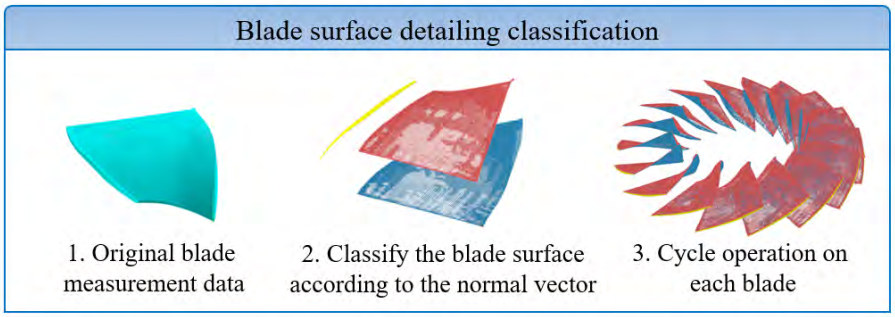

Figure 4 Blade surface detailing classification

To be suitable for large deformation of the finite element mesh, the pressure surface, suction surface ,and top surface of the blade are respectively identified. As shown in the figure, since the top of the blade is an uncertain curved surface, it is hard to distinguish the top surface using the blade PCD coordinates. Therefore, using the normal vector of the plane formed by each triangle as the distinguishing feature, the normal vector calculated on the top surface is different from the others, and the center of gravity formed by the points on the top surface is the farthest from the central axis. These two factors can separate the top surface of the blade. It should be noted that considering the excessive curvature of the root of the blade used by the compressor, the root normal vector will affect the recognition of the top surface. First, cluster analysis of the coordinates of all points of the blade is required to divide the blade into upper and lower segments. The normal vector feature of the upper part of the individual blade is recognized. The cluster analysis method used can be referred to.

0.2.2 Blade edge node processing

The points between the pressure surface, suction surface, top surface are the blade edge points. Use B-spline curves to fit the point cloud edges and take isoparametric points based on finite element edge nodes. The isoparametric point minus the corresponding finite element node is the finite element node movement vector.

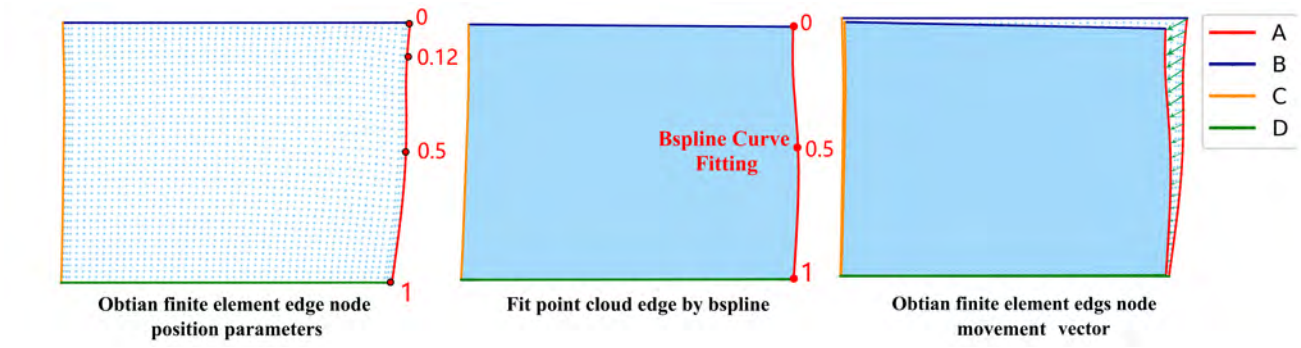

Figure 5 Blade edges nodes fitting method

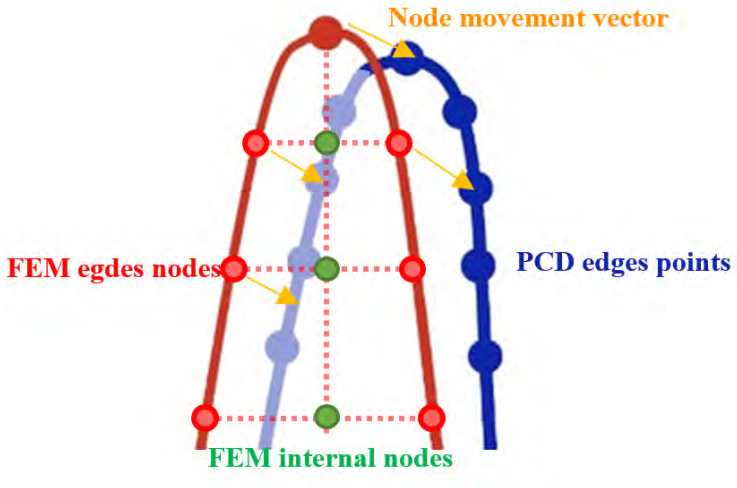

Figure 6 Blade tip node movement vector

In fig6, when the blade edge nodes are moved, too large displacement of the blade tip node will cause the element to be deformed, and the surface is not smooth. After obtaining the movement vector of the edge node, the radial basis function (RBF) is used to allocate these displacements to the adjacent other nodes (FEM internal nodes). The node movement displacements depends on the Euclidean distance between FEM nodes, the specific form of the Gaussian kernel is:

$$K(u,v) = e^{-R/s^2} \tag{7}$$

$$R = \sqrt{\sum (u_i - v_i)^2 / V[x_i]} \tag{8}$$

where the R is the Euclidean distance of the two node vectors, V is the variance vector, and $V[x_i]$ is the variance calculated on the i component of all points.

$$N_i = N_{i-1} + \varphi(r) \otimes K \tag{9}$$

N_{i-1} is the coordinate of the node before moving, N_i is the coordinate of the node after moving, and K is the radial basis matrix of the Gaussian kernel.

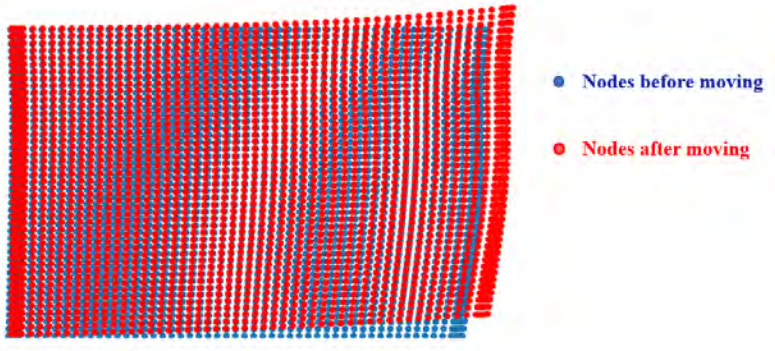

Figure 7 RBF example

In fig7, the blade surface only moves the rightmost edge nodes, and the obtian displacement vector only contains the edge nodes. Using the Gaussian radial basis function can well distribute the edge displacement to other nodes, keeping the original blade surface element shape.

0.3 Blade internal node processing

After moving the finite element edge nodes and assigning the displacemen vectors to other nodes using RBF, the next step is to move the internal nodes of the blade to align with the blade PCD by node normal vectors. Get the node normal

vector through open3d, project the node along the direction of the normal vector and find the PCD triangle that intersects with the normal vector. The idea of the algorithm to determine the intersection of the ray and the triangle is to calculate the intersection point of the ray with the plane where the triangle is located, and then determine whether the intersection point is inside the PCD triangle. For a ray in space, the starting point is O (FEMt node), its ray direction is D (FEM node normal vector), and according to the parameter formula of the ray, any point on it is:

$$N(t) = O + tD \tag{10}$$

where $N(t)$ is the ray, O is the FEM node, D is the Node noraml vector and t is the unknown quantity which can describe any point on the ray. The vertices of the pcd triangle are V_1, V_2, V_3, and the normal vector n in the plane of the triangle. The vectors $-\overline{V_1N(t)}$ and B in the plane of the triangle are perpendicular and the dot product of the them is 0.

$$(V_1 - N(t)) \cdot n = 0 \tag{11}$$

The vertices of the pcd triangle are V_1, V_2, V_3, and the normal vector n in the plane of the triangle. The vectors $-\overline{V_1N(t)}$ and B in the plane of the triangle are perpendicular and the dot product of the them is 0.

$$t = \frac{(V_1 - O) \cdot n}{D \cdot n} \tag{12}$$

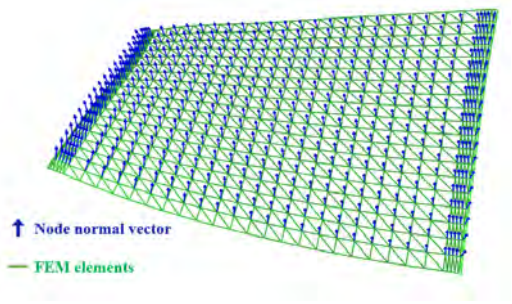

Figure 8 FEM internal node normal vector

0.4 Finite element mesh quality inspections

The accuracy of the finite element analysis depends on the mesh quality, very thin or skewed mesh may lead to inaccurate calculations. Therefore, after using the FEM auto-deformation algorithm, the change in FEM model quality after deformation needs to be checked to determine the validity of the FEM model.

In this paper, the following scoring criterion Durand et al. (2019) is defined to represent the element shape quality in the finite element mesh in the range of 0 to 1, where 0 represents a completely deformed mesh and 1 represents an ideally shaped (standard hexahedron).

$$q(e) = 1 - \left| 1 - \left(\frac{s_r}{s} \right)^2 \right| \tag{13}$$

s is the surface area of a hexahedral unit and s_r is the surface area of a regular hexahedron with the same volume.

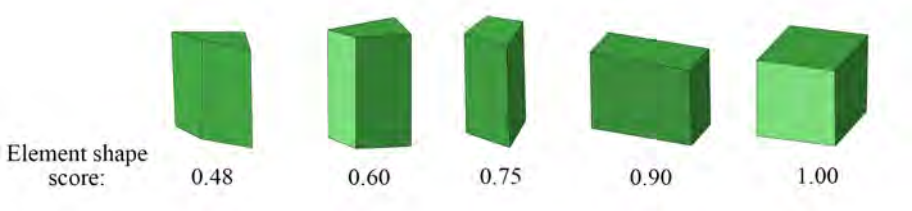

Figure 9 FEM element score

RESULTS AND DISCUSSION

In order to experimentally validate the proposed algorithm, verify the method accuracy as Fig10. A blisk model with the diameter of 320 mm, the modulus of elasticity of 45 Gpa and the density of 7.85 g/cm3 was machined using Computer numerical control(CNC) machine. The blisk has a total of 18 sectors, and the symmetric finite element model divided by the noraml CAD model has a total of 283026 elements and 68579 nodes.

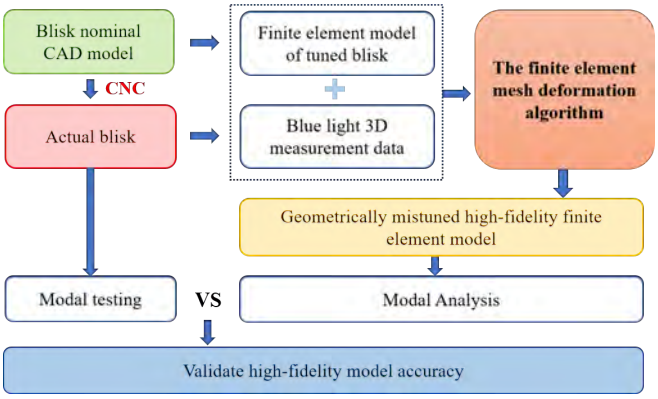

Figure 10 Validation flow chart

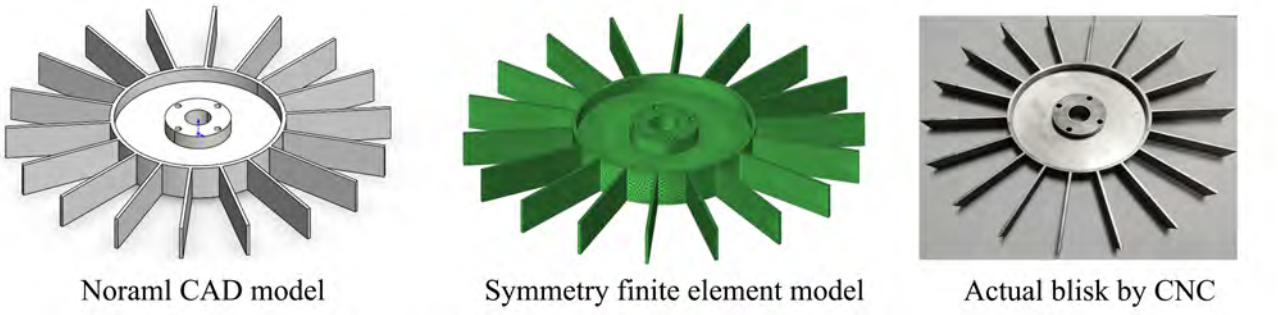

Figure 11 Blisk model

The machined real blisk PCD is obtained by an optical measurement system in Fig12 and includes 582074 points and 1164164 triangles. The high-fidelity mistuned FEM model is established using the automatic FEM mesh deformation algorithm proposed in this paper. The geometric deviation data of the test CNC blisk were characterized, and the mean deviation values of each blade , with the mean values of the blade geometric deviation ranging from 0.008 to 0.022 mm. Fig14 shows the results of the principal component analysis of the 18 blade geometric deviation data, which downscaled the geometric deviation data to a two-dimensional plane, and two groups of outliers (indicated in green and orange, respectively) can be observed. In addition to the similarity of the mean values, the spatial distribution of the two groups of outliers is also distinguished from the other leaves, and there is a similarity between similar outliers.

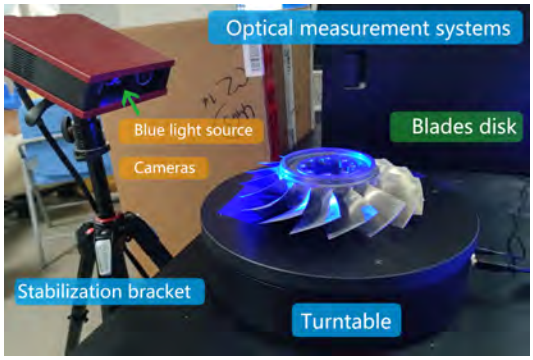

Figure 12 Optical measurement systems

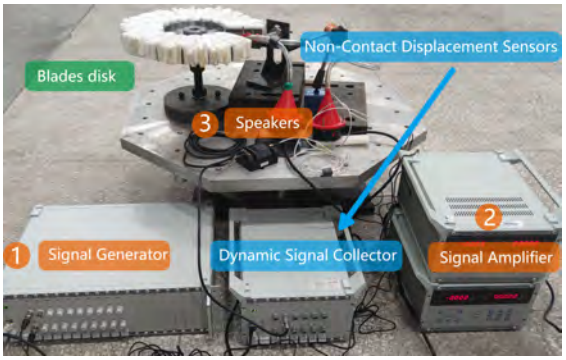

Figure 13 Blade modal excitation test bench

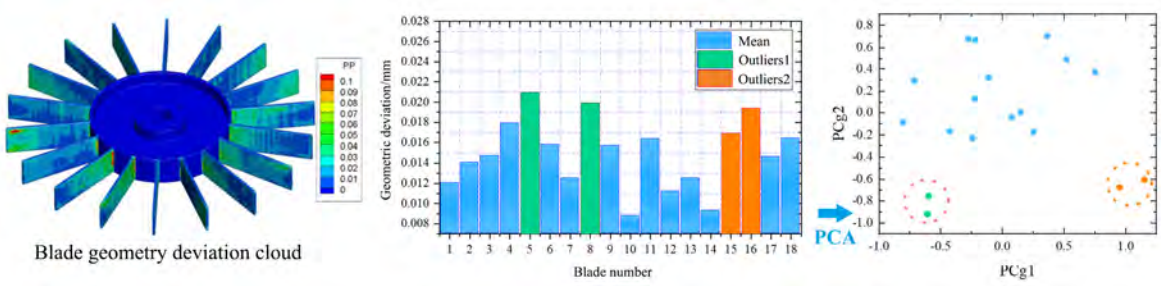

Figure 14 The accumulated energy for first 30th spatial bases in case 1.

Modify the FEM modulus elasticity to the real bladed disk and do the modal analysis of the mistuned high-fidelity FEM model to obtain the natural frequencies of each mistuning blades. The first modal family of blade vibration is dominated by the bending of the blade, and the second modal family of vibration is dominated by the twisting of the blade.

Use blade modal excitation test bench 13 to measure the natural frequencies of each real blade, the system includes a signal generator, a signal amplifier, a loudspeaker as an excitation source, the measurement system including an Non-contanct eddy current displacement sensor, and a dynamic signal collector.

A sinusoidal sweep excitation signal with a fixed sweep speed is fed into the speaker. The acoustic excitation position is the tip of the leading edge of the blade and the blade trailing edge displacement is obtained. The blade displacement is analyzed by short-time Fourier transform(STFT) to obtain the blade frequency and standard deviation of blade frequency obtained from multiple tests is less than 1.

First modal family frequency/Hz	Average	Standard deviation	Coefficient of variation	Min	Max
High fidelity element model	270.383	1.5347	0.00568	267.1743	272.501
Experimental testing	270.41	1.404	0.00519	267.2894	272.267
Second modal family frequency/Hz	Average	Standard deviation	Coefficient of variation	Min	Max
High fidelity element model	1594.735	9.1685	0.00575	1576.215	1608.759
Experimental testing	1595.721	9.0553	0.00567	1576.519	1607.945

Experimental testing data and the analysis result of high fidelity element model are in tabel. Coefficient of variation of mistuning blade frequency is 0.519-0.575, which shows that the degree of mistuning of the high-fidelity mistuning finite element model is very similar to the experimental results. The relative errors of first and second blade modal family frequency between experimental testing to the high fidelity element model are shown in Fig. The relative errors range from 0.107‰ to 2.55‰, and total of 17 blades are below 1‰.

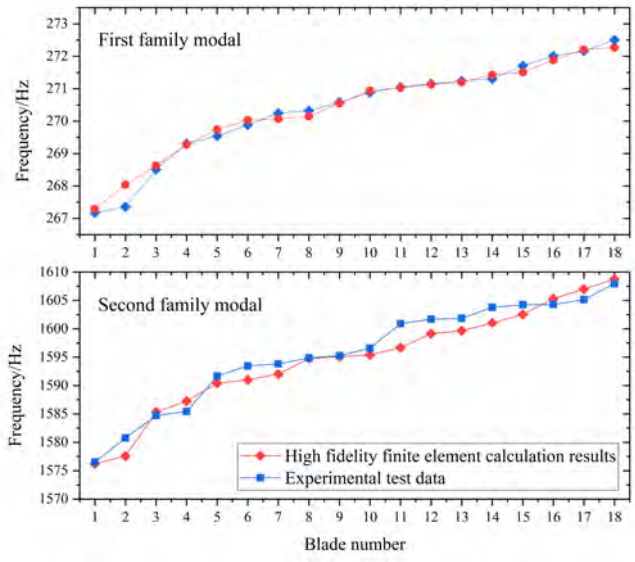

Figure 15 Comparison of experimental results with high-fidelity mistuning model

CONCLUSIONS

The proposed high-fidelity modeling method refines the blue-scanned blade point cloud data and projects the finite element nodes to the PCD, is applicable to various mistuning forms of blades. The quality of the deformed finite element mesh is verified by a mesh quality checker. The high-fidelity modeling accuracy was verified by using modal tests to obtain the intrinsic frequencies of each mistuning blade and comparing them with the computed results of the deformed FEA modal analysis, and the deviation of the high-fidelity model from the test results was <0.8‰ for the first and second modal families of the bladed disk. The mistuning blade high-dimensional geometric data were characterized by PCA which can well differentiate the anomalous blade and describe the geometric deviation using smaller data volume.

REFERENCES

References

Backhaus, T., Harding, M., Schrape, S., Voigt, M. and Mailach, R. (2017), *Validation Methods for 3D Digitizing Precision Concerning Jet Engine BLISKs*, Deutsche Gesellschaft für Luft-und Raumfahrt-Lilienthal-Oberth eV.

Backhaus, T., Maywald, T., Schrape, S., Voigt, M. and Mailach, R. (2017), A parametrization describing blisk airfoil variations referring to modal analysis, *in* 'ASME Turbo Expo 2017: Turbomachinery Technical Conference and Exposition', American Society of Mechanical Engineers Digital Collection.

Boyd, I. M. (2019), 'Adaptive identification of classification decision boundary of turbine blade mode shape under geometric uncertainty'.

Castanier, M. P. and Pierre, C. (2006), 'Modeling and analysis of mistuned bladed disk vibration: current status and emerging directions', *Journal of Propulsion and power* **22**(2), 384–396.

Durand, R., Pantoja-Rosero, B. and Oliveira, V. (2019), 'A general mesh smoothing method for finite elements', *Finite Elements in Analysis and Design* **158**, 17–30.

Harding, K. (2005), Latest optical methods for industrial dimensional metrology, *in* 'Two-and Three-Dimensional Methods for Inspection and Metrology III', Vol. 6000, International Society for Optics and Photonics, p. 600001.

Henry, E. B., Brown, J. M. and Beck, J. A. (2016), Reduced order geometric mistuning models using principal component analysis approximations, *in* '57th AIAA/ASCE/AHS/ASC Structures, Structural Dynamics, and Materials Conference', p. 0706.

Kaszynski, A. A., Beck, J. A. and Brown, J. M. (2014), Automated finite element model mesh updating scheme applicable to mistuning analysis, *in* 'Turbo Expo: Power for Land, Sea, and Air', Vol. 45776, American Society of Mechanical Engineers, p. V07BT33A025.

Kaszynski, A., Brown, J. and Beck, J. (2015), Experimental validation of an optically measured geometric mistuning model using a system id approach, *in* '17th AIAA Non-Deterministic Approaches Conference', p. 1371.

Laxalde, D., Thouverez, F., Sinou, J.-J., Lombard, J.-P. and Baumhauer, S. (2007), 'Mistuning identification and model updating of an industrial blisk', *International Journal of Rotating Machinery* **2007**.

Martel, C. and Corral, R. (2009), 'Asymptotic description of maximum mistuning amplification of bladed disk forced response', *Journal of engineering for gas turbines and power* **131**(2).

Voigt, P., Högner, L., Fiedler, B., Voigt, M., Mailach, R., Meyer, M. and Nasuf, A. (2019), 'Comprehensive geometric description of manufacturing scatter of high-pressure turbine nozzle guide vanes for probabilistic cfd analysis', *Journal of Turbomachinery* **141**(8).